Submonolayer Rare Earth Silicide Thin Films on the Si(111) Surface

S. Sanna, C. Dues, U. Gerstmann, E. Rauls, D. Nozaki, A. Riefer, M. Landmann, M. Rohrmüller, N.J. Vollmers, R. Hölscher, A. Lücke, C. Braun, S. Neufeld, K. Holtgrewe, and W.G. Schmidt

Abstract Rare earth induced silicide phases of submonolayer height and 5×2 periodicity on the Si(111) surface are investigated by density functional theory and ab initio thermodynamics. The most stable silicide thin film consists of alternating Si Seiwatz and honeycomb chains aligned along the $[1\bar{1}0]$ direction, with rare earth atoms in between. This thermodynamically favored model is characterized by a minor band gap reduction compared to bulk Si and explains nicely the measured scanning tunneling microscopy images.

1 Introduction

Metallic rare earth (RE) silicides can be grown epitaxially as thin films on the Si(111) substrate by rare earth deposition and thermal treatment [1–3]. The resulting metal/semiconductor interface is characterized by an extraordinarily low Schottky barrier height of 0.3–0.4 eV on *n*-type substrates. Due to the marginal lattice mismatch [4] between substrate and thin film, the interface furthermore has a low defect concentration and is very stable. Therefore rare earth silicides on *n*-type silicon are considered ideal candidates for Ohmic contacts [5, 6]. The relatively high barrier height on *p*-type substrates makes them interesting for infrared detectors and photovoltaic applications [7]. For submonolayer coverage, a variety of structures with different periodicities was found [8–12].

Despite the large and growing interest in silicide thin films on Si(111), our knowledge of these systems is still fragmentary. A multitude of surface reconstructions or nanostructures with different periodicities has been observed, depending on the rare earth species and rare earth coverage [8–19]. The observed structures are characterized by different stoichiometries and heights. For the case of dysprosium silicide, e.g., a full monolayer results in a film with 1×1 periodicity and $DySi_2$ hexagonal structure, multilayer silicides grow in a film with $\sqrt{3} \times \sqrt{3}$ periodicity

S. Sanna (✉) • C. Dues • U. Gerstmann • E. Rauls • D. Nozaki • A. Riefer • M. Landmann • M. Rohrmüller • N.J. Vollmers • R. Hölscher • A. Lücke • C. Braun • S. Neufeld • K. Holtgrewe • W.G. Schmidt
Lehrstuhl für Theoretische Physik, Universität Paderborn, 33095 Paderborn, Germany
e-mail: simone.sanna@uni-paderborn.de

W.E. Nagel et al. (eds.), *High Performance Computing in Science and Engineering '16*, DOI 10.1007/978-3-319-47066-5_12

and Dy_3Si_5 composition, while submonolayer coverage results in structures with $2\sqrt{3} \times 2\sqrt{3}$ or 5×2 periodicity [10].

Computational studies of two-dimensional rare-earth silicides are rare and limited to the simplest yttrium and erbium silicide structures [15, 18–23]. The lack of theoretical investigations is particularly severe in the submonolayer range, where, to the best of our knowledge, no theoretical investigations are available.

The present paper aims at providing microscopic structural models for the silicide thin film 5×2 phase observed in the submonolayer regime. To this end, we combine total energy density functional theory (DFT) calculations with ab initio thermodynamics. Calculations are performed using Tb (atomic number 65) and Dy (atomic number 66) as prototypical trivalent rare earths.

2 Methodology

Total-energy density functional theory (DFT) calculations are performed within the generalized gradient approximation [24] (GGA) in the Perdew-Burke-Ernzerhof formulation [25] as implemented in the Vienna ab initio simulation package (VASP) [26, 27]. Projector augmented wave [28, 29] (PAW) potentials with projectors up to $l = 1$ for H, $l = 2$ for Si and $l = 3$ for the rare earth atoms, as well as a plane wave cutoff of 400 eV have been used. As no other valence state than RE^{3+} has been observed for the rare earth ions in the silicide structures, we constrain the valence state of the investigated rare earth ions treating f electrons as core states. This approach, commonly referred to as frozen-core method, allows for a proper treatment of the lanthanides within DFT [30–32].

Six Si bilayers stacked along the [111] crystallographic direction model the substrate. The periodic supercell contains in addition the silicide thin film of variable structure and height, and a vacuum region of at least 15 Å. The dangling bonds at the bottom of the slab are saturated by H atoms. The atomic positions are relaxed until the residual Hellmann-Feynman forces are lower than 0.001 eV/Å. Thereby three Si bilayers and the hydrogen atoms are kept frozen. Test calculations show that adding further substrate layers does not result in noticeable changes of the calculated geometries and band structures. Dipole-correction algorithms have been used to correct the spurious interactions of the slabs with their periodic images [33, 34].

Simulated constant-current STM images are calculated within the Tersoff-Hamann approach [35, 36] on the basis of the partial densities of states (LDOS).

In order to compare the formation energy of silicide films with different composition, we use the Landau potential Ω, approximated as [37, 38]

$$\Omega(\mu_{\mathrm{Si}}, \mu_{\mathrm{RE}}) \approx E^{DFT}(N_{\mathrm{Si}}, N_{\mathrm{RE}}) - \sum_{i}^{\mathrm{Si,RE}} \mu_i N_i. \tag{1}$$

In this equation, $E^{DFT}(N_{\mathrm{Si}}, N_{\mathrm{RE}})$ is the DFT total energy of a slab containing N_{Si} silicon atoms and N_{RE} rare earth atoms. μ_{Si} and μ_{RE} are the corresponding chemical potentials and represent the experimental growth conditions. The sum in Eq. 1 also extends to the H atoms employed to saturate the Si dangling bonds at the bottom side of the slabs. The usage of the total rather than the free energy for the calculation of Ω is an approximation. It is justified as long as the entropic contributions are of similar magnitude for the different silicide films.

The Landau potential Ω in Eq. 1 is expressed as a function of the chemical potentials μ_{Si} and μ_{RE}. Their thermodynamically allowed range is constrained by several conditions. The upper limits are given by the bulk phases,

$$\mu_{\mathrm{i}} \leq \mu_{\mathrm{i}}^{\mathrm{bulk}} \quad i = \mathrm{Si}, \mathrm{RE}. \tag{2}$$

Furthermore the silicide films are in equilibrium with the Si substrate, which represents an infinite reservoir of Si atoms. This pins the value of μ_{Si} to $\mu_{\mathrm{Si}}^{\mathrm{bulk}}$ and allows to express the Landau potential as $\Omega = \Omega(\mu_{\mathrm{RE}})$. The RE chemical potential can be controlled experimentally with the amount of rare earth deposited on the Si substrate before annealing. If we restrict our investigation to silicide phases with a given stoichiometry $\mathrm{RE}_\alpha\mathrm{Si}_\beta$, the lower limit of μ_{RE} is given by

$$\alpha \cdot \mu_{\mathrm{Si}}^{\mathrm{bulk}} + \beta \cdot \mu_{\mathrm{RE}} = \mu_{\mathrm{Si}_\alpha\mathrm{RE}_\beta}^{\mathrm{bulk}} \tag{3}$$

where we use $\mu_{\mathrm{Si}} = \mu_{\mathrm{Si}}^{\mathrm{bulk}}$ as we consider Si rich conditions. However, we also consider lower values of μ_{RE}, representing non-stoichiometric silicides with dilute rare earth concentrations.

The values of the bulk chemical potentials are estimated by the total energy per formula unit calculated within DFT using hexagonal stoichiometric RESi_2 phases with AlB_2 structure (space group D_{3d}^3) for the silicides, hexagonal close-packed structures (space group D_{6h}^4) for the metallic elemental rare earths and the gas phase of hydrogen.

Highly customizable parallelization schemes are implemented in VASP. In particular, parallelization (and data distribution) over bands, parallelization (and data distribution) over plane wave coefficients, as well as parallelization over k-points (no data distribution) can to be used at the same time on massively parallel systems such as the Cray XC40 (Hazel Hen), in order to obtain high computational efficiency.

The performance of the Cray XC40 in combination with the available parallelization routines has been tested and optimized with VASP 5.3.5 and a test system consisting of 1620 electrons distributed over 1120 orbitals of different symmetry.

The first step of the parallelization procedure is the distribution of the workload related to each orbital on a certain number of cores. It turns out that a number of cores corresponding approximately either to the square root of all available cores or to the number of cores per node works best for the HRLS Hazel Hen. In addition, this method significantly improves the stability due to reduced memory

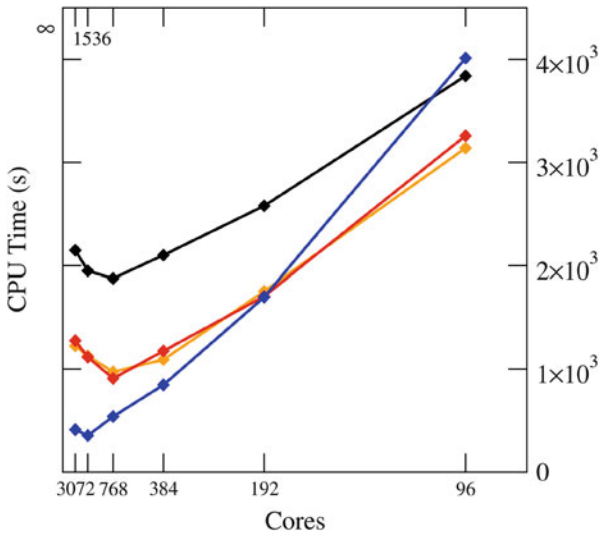

Fig. 1 CPU time on the HRLS CRAY XE6 for the self consistent calculation of the electronic structure of a $LiNbO_3$ slab within different parallelization schemes. See text for details

requirements. Numerical results for the test configuration are shown in Fig. 1 (red line). This setup results in a roughly linear scaling up to 768 cores.

Within the described approach for parallel computing, it is possible to steer the data distribution mode. In particular, the plane wise data distribution in real space can be activated. This allows for a much reduced communication during the Fourier transforms (FFTs). Unfortunately, the resulting load balancing is worsened. Therefore, the suitability of the plane wise data distribution must be tested for the particular computational architecture and in dependence of the number of processors. The results of our tests are shown in Fig. 1 (orange line). As expected, advantages of the plane wise data distribution occur for a relatively small numbers of processors, but are outweighted by load-balancing problems for calculations that employ 768 cores.

The computational techniques for the modeling of atomic system discussed here rely on mathematical libraries, in particular the Linear Algebra Package LAPACK or its distributed-memory implementation ScaLAPACK. The calculations discussed above have been performed with ScaLAPACK. This speeds up the calculations by up to a factor of two compared to LAPACK calculations, shown by the black line in Fig. 1. Even if only 96 cores are used, there is a noticeable speed up achieved by using the scalable linear algebra package.

Starting with VASP Version 5.3.2 it is possible to use additionally a parallelization over the k points used to sample the Brillouin zone in the reciprocal space calculations. Thereby it is possible to specify the number of k points that are to be treated in parallel. Within the group of cores that share the work for an individual k point also the electronic states and/or plane wave coefficients are treated in parallel.

The results of the corresponding tests are shown in Fig. 1 (blue line). It can be seen that the k point parallelization leads to an additional saving of computer time, provided more than 192 cores are used. The speed up with respect to calculations without k point parallelization amounts up to a factor two. Moreover, this approach allows for the extension of the roughly linear scaling to 1536 cores.

3 Results

The Si(111) surface reconstructs 2×1 if cleaved at room temperature. Annealing at 400 °C leads to a superstructure with a 7×7 periodicity [39]. However, since rare earth adsorbates typically prevent the formation of these surface reconstructions, we focus on the unreconstructed Si(111) surface. It is characterized by a hexagonal surface unit cell. Cutting bulk Si perpendicularly to the [111] crystallographic directions results in broken sp^3 bonds at the topmost Si layer, creating one dangling bond per surface unit cell. Indeed, the corresponding surface band structure shows a single surface state localized within the electronic band gap. The band is half filled and crosses the Fermi level.

During the silicide growth process, rare earth ions are deposited at the Si(111) surface. In order to identify the energetically favorable adsorption sites, we have calculated the potential energy surface for the adsorption of isolated atoms at the Si(111) 1×1 surface. It is calculated constraining the lateral coordinates of the rare earth atom and allowing its height as well as the remaining degrees of freedom of the uppermost three Si substrate bilayers to relax. We determined the energy for 56 lateral positions on a rectangular grid (average spacing 0.5 Å). The energy between the grid points is then evaluated by bicubic interpolation of the calculated data. The outcome of our calculation in the case of Dy is shown in Fig. 2. The rare earth ion prefers adsorption at the hcp site (T_4, global minimum) or at the fcc site (H_3, local minimum). The energy difference between the two sites amounts to 225 meV, and the low energy barrier between the two minima (about 300 meV) indicates a relatively high mobility of the adsorbates.

5×2 silicide phases of Gd, [11, 40] Tb, [12] Dy, [10] Ho, [41] and Er [42] have been recently observed by STM. This structure consists of a silicide submonolayer termination and is – exactly as the $2\sqrt{3} \times 2\sqrt{3}$ phase – metastable [42]. The two structures are in competition at low rare earth coverage. However, both are transformed into more stable silicides upon annealing. Available STM images reveal chain-like structures in the $[1\bar{1}0]$ direction (three equivalent chain orientations are thus possible).

However, without precise knowledge of the rare earth content, it is hard to extract structural information from the STM images. Consequently, very few attempts to assign a structural model to the rare earth film are available in the literature [11, 12].

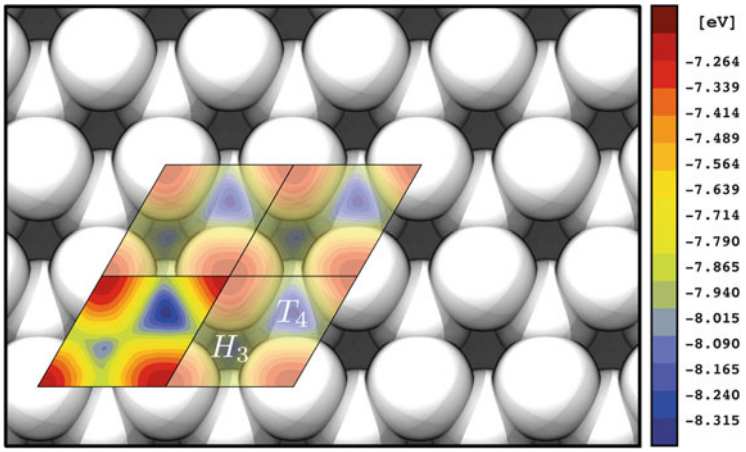

Fig. 2 Calculated potential energy surface for a single Dy atom at Si(111)

In order to develop a model for the 5×2 superstructure, several factors can be considered. First of all, the stable silicides depend on the lanthanide coverage. In detail, $2\sqrt{3} \times 2\sqrt{3}$, 5×2 and finally the 1×1 surface periodicity is observed with increasing rare earth availability. Considering the size of the respective surface unit cells, this limits the number of rare earth atoms to a maximum of 10 atoms per surface unit. Furthermore, available STM images reveal the presence of ordered chains along the $[1\overline{1}0]$ direction. Thus the rare earth atoms are placed in our models in the stable positions determined in above, so that oriented chain-like structures are formed. As the rare earth atoms in silicide films with 1×1 periodicity are completely covered by a silicon double layer that is absent in the films with $2\sqrt{3} \times 2\sqrt{3}$ periodicity, it is plausible that the lanthanide ions in the 5×2 phase are at least partially covered by Si atoms. Therefore, rare earth layers covered to a different extent are simulated. In order to capture possible Si dimerization effects as known from other silicon surfaces – e.g the Si(001) – doubled 5×1 unit cells with artificial dimerization in the $[1\overline{1}0]$ directions are employed. Models consisting of alternating Si Seiwatz and honeycomb chains with rare earth atoms in between, as originally proposed by Battaglia et al. [11] and then by Franz et al. [12], have been tested as well.

Following the criteria above, we have developed 14 structural models, which are shown in Figs. 3 and 5. Besides the labels *a* to *n*, corresponding to Fig. 3a–n, the number of rare earth atoms per 5×2 unit cell is indicated in the picture. While certainly further models are conceivable, the models described above are expected to allow for the derivation of general trends and conclusions. As the slabs modeling the surface structures contain a different number of Si and rare earth atoms, their DFT total energy cannot be directly compared. In order to determine the thermodynamically stable structures, we calculate the Landau potential as described in Sect. 2. As neither the contribution to the free energy of the hydrogen atoms

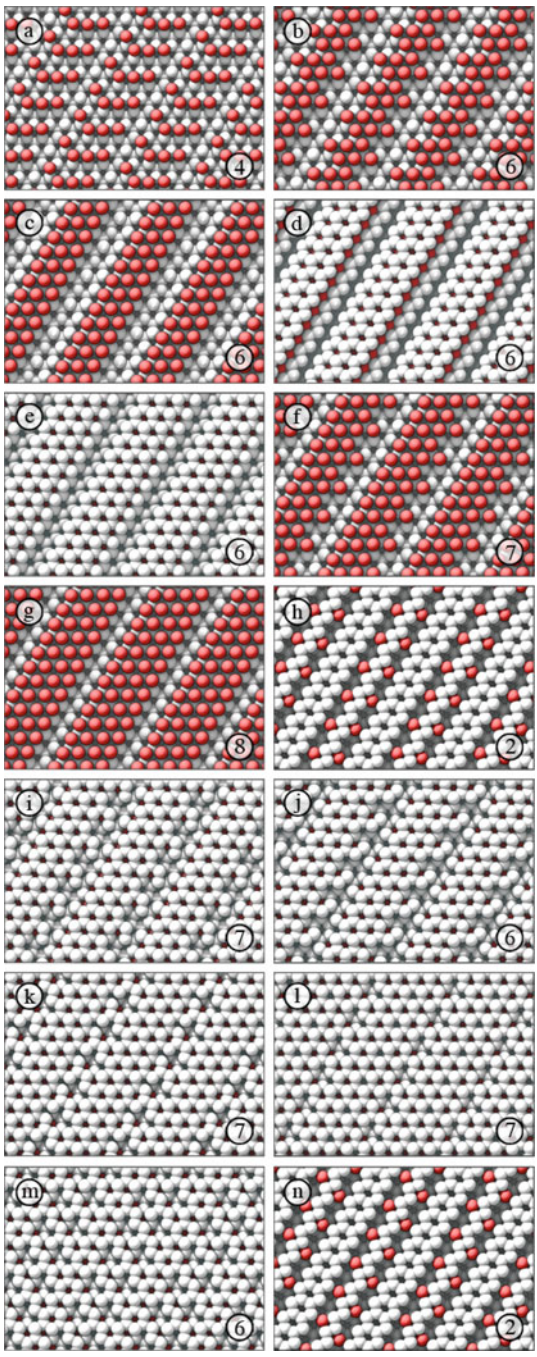

Fig. 3 Structural models for RE induced Si(111)(5 × 2) surface reconstructions. Numbers in the *lower right corner* indicate the number of RE atoms per unit cell

nor the size of the surface unit cell are considered for this particular calculation, the calculated values do not correspond to the absolute formation energies of the structures and the Landau potential is labeled by Ω'. However, as both the surface unit cell as well as the number of hydrogen atoms used to passivate the dangling bonds at the bottom side of the slabs are the same for all configurations, a relative comparison of the different structures is possible. Even if the 5×2 phase has been observed for different rare earth silicides, we limit our investigation to Dy silicide due to the high demand of computational resources. However, based on our experience with the other silicide structures discussed above, the results may again be extrapolated to all trivalent rare earths.

The phase diagram in Fig. 4 shows that structures with rare earth atoms in the channels between honeycomb and Seiwatz chains (*h*, *n*) are favored. Indeed, for most values of the chemical potentials, which are relevant for submonolayer coverage, the structures labeled by *h* and *n* are the most stable configurations, while for strongly Dy rich conditions the models *m* and *i* can be formed. These structures are less relevant, however, since at these values of the rare earth chemical potential monolayer or multilayer silicides are formed.

Thus, the energetically almost degenerate models *h* and *n* (energy difference 18 meV per 5×2 unit cell) with two rare earth atoms per unit cell describe the observed phase. Considering that four and eight Si atoms per 5×2 unit cell form the Seiwatz and honeycomb chains, respectively, the stoichiometry of the silicide layer at the Si(111) surface can be expressed as $RESi_6$. The difference between the two

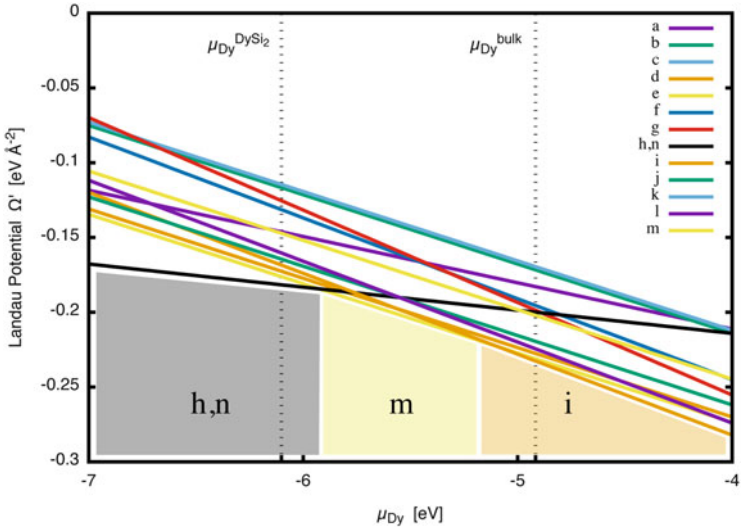

Fig. 4 Calculated phase diagram for the dysprosium adsorbed Si(111) surface with 5×2 periodicity as a function of the dysprosium chemical potential μ^{Dy}. Two representative values of μ^{Dy}, corresponding to Dy in its metallic hcp bulk phase and to Dy in hexagonal $DySi_2$ state are indicated. Si-rich conditions are assumed

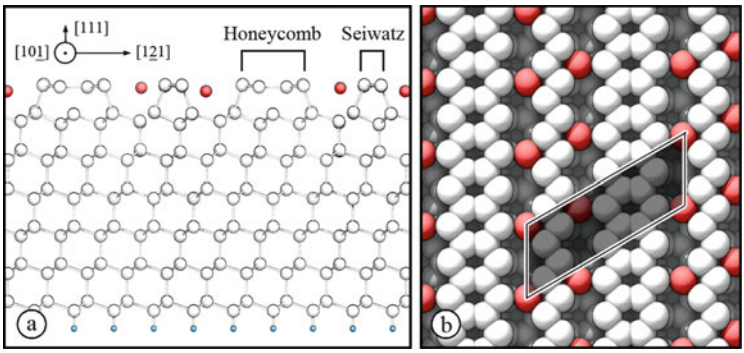

Fig. 5 Side (**a**) and top view (**b**) of the thermodynamically stable rare earth induced surface reconstruction with 5 × 2 periodicity on the Si(111) surface. The termination corresponds to structure *h* in Figs. 3 and 4 and consists of alternating Si Seiwatz and honeycomb chains. The surface unit cell is highlighted

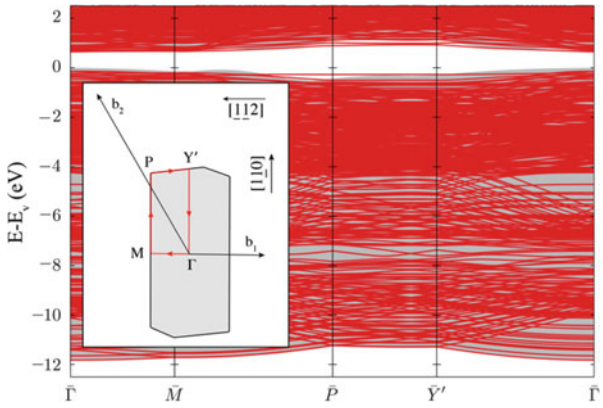

Fig. 6 Calculated surface band structure for model *h* in Figs. 3 and 4. Projected bulk bands are shown in *grey*. The *inset* shows the surface Brillouin zone of the 5 × 2 structure

models *h* and *n* consists in the different alignments of neighboring rare earth atom rows on both sides of the honeycomb chains. The slightly more stable model *h*, in which the rare earth atoms are aligned in-phase, is shown in more detail in Fig. 5. It is known that on Si(111) a honeycomb chain is stabilized by one electron per 3 × 1 unit cell, while a zigzag Seiwatz chain requires two electrons per 2 × 1 unit cell [11]. Thus, the 5 × 2 phase is built of two 3 × 1 surface units with honeycomb chains and two 2 × 1 surface units containing Seiwatz chains. The structure is stabilized by two trivalent rare earth atoms, which provide six electrons per unit cell.

Figure 6 shows the calculated electronic band structure of model *h*. We mention that the Si bulk band gap calculated here is about 0.67 eV i.e. slightly smaller than measured, due to the underestimation of the band gaps in DFT calculations [37]. Almost no surface localized electronic states are present in the bulk gap region. The

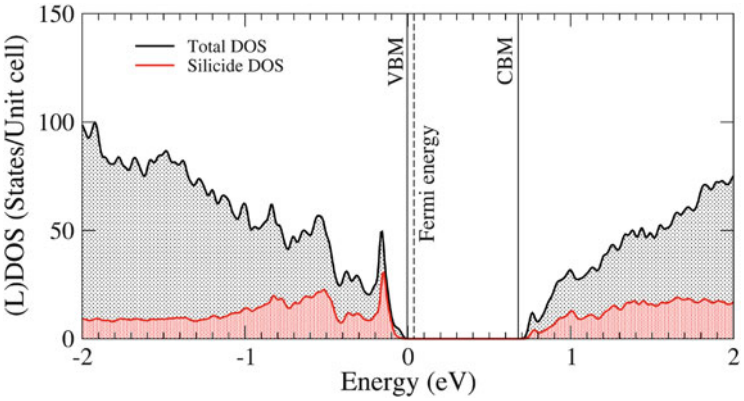

Fig. 7 Calculated density of states for model *h* in Figs. 3 and 4. The total density of states is shown *black*, while the silicide contribution is shown *red*

fundamental electronic gap (direct, at $\overline{\Gamma}$) is only slightly smaller than the calculated Si bulk gap. This confirms that the submonolayer silicide with 5×2 periodicity on the Si(111) surface is semiconducting. The inset of Fig. 6 shows the 5×2 surface Brillouin zone employed for the calculations. The atomic chains are parallel to the long sides of the surface Brillouin zone.

The (local) density of states of the slab modeling the $DySi_6$ silicide with 5×2 periodicity on the Si(111) surface is shown in Fig. 7. The total density of states is represented by the black curve, while the red curve represents the local DOS of the silicide layer. The dotted lines indicate the valence and conduction band edges of bulk Si. The calculated (L)DOS again shows that the silicide layer is semiconducting. The overall appearance of the total DOS is very similar to the Si bulk DOS, with the exception of a minor reduction of the fundamental bandgap. This effect is due to the electronic states close to the conduction band minimum. Otherwise the presence of the $DySi_6$ layer does not strongly affect the band gap region of the substrate.

The knowledge of the thermodynamically stable structural model now also allows for the interpretation of the STM images and the identification of the observed features. In the filled state images (Fig. 8a, c) the bright spots are assigned to the honeycomb (broad rows) and Seiwatz (thin rows) chains, which capture the electrons from the rare earth atoms. The latter are thus not visible at this bias. In contrast, in the empty state images (Fig. 8b, d), the rare earth atoms donating their electrons are visible, while the dark rows show the location of the honeycomb chains. As between the chains different equivalent lattice sites are available for the rare-earth atoms, different STM patterns are possible. These correspond to an in-phase alignment between neighboring rare earth rows (model *h*) or a zigzag alignment (model *n*).

In contrast to monovalent and divalent ions, for which also other $n \times 2$ phases with odd $n \neq 5$ have been observed, 5×2 is the only possible $n \times 2$ periodicity for

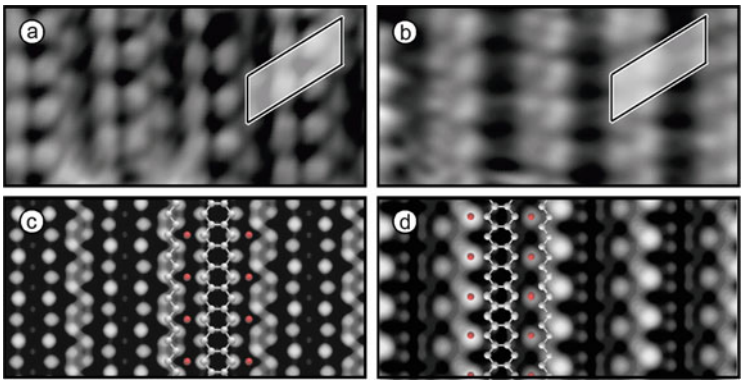

Fig. 8 (**a**), (**b**) Measured STM images of the 5 × 2 Tb silicide submonolayer structure on the Si(111) surface [12] in comparison with simulated data in (**c**), (**d**). Experimental STM images refer to voltages of −1.5 V [(**a**), (**c**) filled states] and 1.5 V [(**b**), (**d**) empty states], and tunneling currents of 100 pA. The 5 × 2 surface unit cell is indicated

trivalent rare earths.[1] Sticking to the models consisting of alternating honeycomb and Seiwatz chains, phases of 7 × 2 or 9 × 2 periodicity could in principle be built by one honeycomb chain and two or three Seiwatz chains, respectively. These structures, however, would have to be stabilized by 10 and 14 electrons per unit cell, respectively. This condition cannot be satisfied by an integer number of trivalent donors, which explains why no other $n \times 2$ phase than the 5 × 2 has been observed for trivalent rare earths.

4 Conclusions

Two-dimensional silicide structures of 5×2 periodicity formed at the Si(111) surface upon rare earth deposition in the submonolayer regime have been investigated theoretically. The DFT calculations allow for the identification of a structural model that is compatible with the experimental data.

According to this model, the 5 × 2 structure is characterized by alternating Si honeycomb and Seiwatz chains oriented along the $[10\bar{1}]$ crystallographic direction. The rare earth atoms are located in the channels between the chains. The formation

[1] It is also important to notice that the adsorption of divalent metals at the Si(111) typically leads to a $n \times 2$ surface reconstruction, with n an odd integer. Thus, as suggested by Battaglia et al. [11], the 5 × 2 phase might be induced by divalent lanthanides such as Yb, Eu, Sm or Tm. In this case, they would give rise to completely different structures, similar to the reconstructions formed by deposition of divalent alkaline-metal earths (Mg, Ca, Sr, Ba). These are not investigated in this work, as we only consider lanthanides in the trivalent state (Dy^{3+},Tb^{3+}).

of the silicide structures with 5×2 periodicity does not strongly affect the electronic properties of the substrate, but slightly reduces the band gap.

Acknowledgements The Deutsche Forschungsgemeinschaft (DFG) is acknowledged for financial support (FOR1700, SCHM 1361/21). The calculations were performed at the High Performance Computing Center Stuttgart (HLRS) and the Paderborn Center for Parallel Computing (PC^2).

References

1. Paki, P., Kafader, U., Wetzel, P., Pirri, C., Peruchetti, J.C., Bolmont, D., Gewinner, G.: Phys. Rev. B **45**, 8490 (1992)
2. d'Avitaya, F.A., Perio, A., Oberlin, J.C., Campidelli, Y., Chroboczek, J.A.: Appl. Phys. Lett. **54**(22), 2198 (1989)
3. Knapp, J.A., Picraux, S.T.: Appl. Phys. Lett. **48**(7), 466 (1986)
4. Wetzel, P., Pirri, C., Paki, P., Peruchetti, J., Bolmont, D., Gewinner, G.: Solid State Commun. **82**(4), 235 (1992)
5. Tu, K.N., Thompson, R.D., Tsaur, B.Y.: Appl. Phys. Lett. **38**(8), 626 (1981)
6. Vandré, S., Preinesberger, C., Busse, W., Dähne, M.: Appl. Phys. Lett. **78**(14), 2012 (2001)
7. Vandré, S., Kalka, T., Preinesberger, C., Dähne-Prietsch, M.: Phys. Rev. Lett. **82**, 1927 (1999)
8. Lohmeier, M., Huisman, W.J., ter Horst, G., Zagwijn, P.M., Vlieg, E., Nicklin, C.L., Turner, T.S.: Phys. Rev. B **54**, 2004 (1996)
9. Roge, T., Palmino, F., Savall, C., Labrune, J., Pirri, C.: Surf. Sci. **383**(2–3), 350 (1997)
10. Engelhardt, I., Preinesberger, C., Becker, S., Eisele, H., Dähne, M.: Surf. Sci. **600**(3), 755 (2006)
11. Battaglia, C., Cercellier, H., Monney, C., Garnier, M.G., Aebi, P.: EPL (Europhys. Lett.) **77**(3), 36003 (2007)
12. Franz, M., Große, J., Kohlhaas, R., Dähne, M.: Surf. Sci. **637–638**, 149 (2015)
13. Wanke, M., Franz, M., Vetterlein, M., Pruskil, G., Höpfner, B., Prohl, C., Engelhardt, I., Stojanov, P., Huwald, E., Riley, J., Dähne, M.: Surf. Sci. **603**(17), 2808 (2009)
14. Wanke, M., Franz, M., Vetterlein, M., Pruskil, G., Prohl, C., Höpfner, B., Stojanov, P., Huwald, E., Riley, J.D., Dähne, M.: J. Appl. Phys. **108**(6), 064304 (2010)
15. Stauffer, L., Mharchi, A., Pirri, C., Wetzel, P., Bolmont, D., Gewinner, G., Minot, C.: Phys. Rev. B **47**, 10555 (1993)
16. Kitayama, H., Tear, S., Spence, D., Urano, T.: Surf. Sci. **482–485**(Part 2), 1481 (2001)
17. Bonet, C., Spence, D., Tear, S.: Surf. Sci. **504**, 183 (2002)
18. Rogero, C., Koitzsch, C., González, M.E., Aebi, P., Cerdá, J., Martín-Gago, J.A.: Phys. Rev. B **69**, 045312 (2004)
19. Rogero, C., Martín-Gago, J.A., Cerdá, J.I.: Phys. Rev. B **74**, 121404 (2006)
20. Koitzsch, C., Bovet, M., Garnier, M., Aebi, P., Rogero, C., Martín-Gago, J.: Surf. Sci. **566–568**(Part 2), 1047 (2004) (Proceedings of the 22nd European Conference on Surface Science)
21. Magaud, L., Reinisch, G., Pasturel, A., Mallet, P., E. Dupont-Ferrier, Veuillen, J.Y.: EPL (Europhys. Lett.) **69**(5), 784 (2005)
22. Wetzel, P., Saintenoy, S., Pirri, C., Bolmont, D., Gewinner, G.: Phys. Rev. B **50**, 10886 (1994)
23. Cocoletzi, G.H., de la Cruz, M.R., Takeuchi, N.: Surf. Sci. **602**(2), 644 (2008)
24. Perdew, P., Chevary, J.A., Vosko, S.H., Jackson, K.A., Pederson, M.R., Singh, D.J., Fiolhais, C.: Phys. Rev. B **46**, 6671 (1992)
25. Perdew, J.P., Burke, K., Ernzerhof, M.: Phys. Rev. Lett. **77**, 3865 (1996)
26. Kresse, G., Furthmüller, J.: Comput. Mater. Sci. **6**, 15 (1996)
27. Kresse, G., Furthmüller, J.: Phys. Rev. B **54**, 11169 (1996)
28. Bloechl, P.E.: Phys. Rev. B **50**(24), 17953 (1994)

29. Kresse, G., Joubert, D.: Phys. Rev. B **59**, 1758 (1999)
30. Anisimov, V.I., Aryasetiawan, F., Lichtenstein, A.I.: J. Phys. Condensed Matter **9**(4), 767 (1999)
31. Sanna, S., Schmidt, W.G., Frauenheim, T., Gerstmann, U.: Phys. Rev. B **80**, 104120 (2009)
32. Sanna, S., Frauenheim, T., Gerstmann, U.: Phys. Rev. B **78**, 085201 (2008)
33. Neugebauer, J., Scheffler, M.: Phys. Rev. B **46**(24), 16067 (1992)
34. Bengtsson, L.: Phys. Rev. B **59**(19), 12301 (1999)
35. Tersoff, J., Hamann, D.R.: Phys. Rev. Lett. **50**, 1998 (1983)
36. Tersoff, J., Hamann, D.R.: Phys. Rev. B **31**, 805 (1985)
37. Bechstedt, F.: Principles of Surface Physics. Advanced Texts in Physics. Springer, Berlin/Heidelberg (2003)
38. Sanna, S., Schmidt, W.G.: Phys. Rev. B **81**(21), 214116 (2010)
39. Lüth, c: Surfaces and Interfaces of Solid Materials. Springer Study Edition. Springer, Berlin/Heidelberg (1995)
40. Kirakosian, A., McChesney, J., Bennewitz, R., Crain, J., Lin, J.L., Himpsel, F.: Surf. Sci. **498**(3), L109 (2002)
41. Perkins, E., Scott, I., Tear, S.: Surf. Sci. **578**(1–3), 80 (2005)
42. Wetzel, P., Pirri, C., Gewinner, G., Pelletier, S., Roge, P., Palmino, F., Labrune, J.C.: Phys. Rev. B **56**, 9819 (1997)